PIER C

Design and Optimization of Reverse Series Triple Coil Structure with Simultaneous Offset and Load Fluctuation Resistance

Xiaohua Shu[1], Jianbin Wang[1], Chenxi Zhang[1], and Zhongqi Li[1, 2, 3, *]

[1]*College of Railway Transportation, Hunan University of Technology, Zhuzhou 412007, China*
[2]*College of Electrical and Information Engineering, Hunan University, Changsha 412008, China*
[3]*College of Electrical and Information Engineering, Hunan University of Technology, Zhuzhou 412007, China*

ABSTRACT: In wireless power transfer (WPT) systems, the horizontal misalignment between coils and variations in the load result in significant fluctuations in the transmission efficiency of the system. In this paper, a reverse series triple coil (RTC) structure is proposed. The RTC structure offers improved resistance to deflection in the direction of vehicle motion because of the magnetic field interaction of the reverse series coils. This adjustment helps maintain a more stable system transmission efficiency when the coils are deflected. At the same time, when the load resistance varies within a certain range, the system's transmission efficiency remains almost unchanged. This is because the addition of relay coils makes the system more adaptable to load changes and improves the system's load compatibility. The experimental results indicate that the RTC structure corresponds to 300% of the load variation range of the conventional reverse series dual-coil structure, within the range where the system transmission efficiency is not less than 95%, in the load variation range that satisfies the load equivalent resistance from $15\,\Omega$ to $68\,\Omega$. During the offset process, the maximum system transmission efficiency fluctuation rate is 1.19% for a distance of 55% of the core width of the offset transmitting coil on the horizontal Y-axis, and the maximum efficiency reaches as high as 97.26%.

1. INTRODUCTION

Compared with the traditional wired electrical power transmission methods, wireless power transmission has many advantages such as high flexibility, convenience, and no need for physical contact, which makes it a potential solution to many challenges in energy transmission [1, 2]. Wireless power transfer can be categorized into static wireless charging (SWC) [3–5] and dynamic wireless charging (DWC) [6–8] methods. Static wireless power transmission refers to the charging method of wireless power transmission in a fixed location or a specific area. This method is suitable for some low-power devices or scenarios that require charging in a fixed location. Dynamic wireless power transfer is a charging method that occurs at the receiving side, which is suitable for mobile devices or electric vehicles. Dynamic wireless charging technology can mitigate the effect of distance limitation of electric vehicles caused by insufficient battery capacity [9]. In the process of dynamic wireless charging, when the receiving coil (R_x) passes 50% of the length of the transmitting coil (T_x) in sequence, the former transmitting coil stops working, and the latter transmitting coil starts running, so as to achieve a mobile charging effect through the mutual articulation between the transmitting coils [10, 11]. The schematic diagram of dynamic wireless charging is shown in Figure 1.
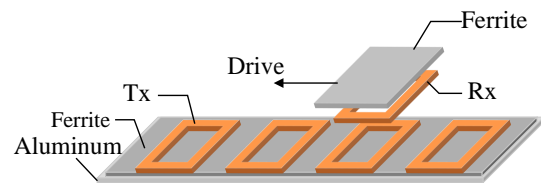
FIGURE 1. Schematic of dynamic wireless power transmission

In dynamic wireless charging technology, as an electric vehicle travels horizontally in the direction of motion, the receiving coil at the bottom of the vehicle is horizontally offset above the short-track transmitting coil, which leads to an unavoidable edge position of the transmitting and receiving coils. Existing coil structures have poor quasi-constant efficiency, and the wireless power transmission system is less efficient when it is in the edge position, leading to larger fluctuations in the system transmission efficiency. Moreover, the transmission efficiency of a wireless power transmission system is highly dependent on the impedance matching between the transmitting and receiving coils. Varied load resistance values lead to impedance mismatch, which impacts the transmission efficiency of the system. In the existing wireless power transmission systems for electric vehicles, the vast majority of coil structures are characterized by incompatibility with load variations, which makes the production of coil structures in wireless power transmission systems for electric vehicles too specialized for mass production.

* Corresponding author: Zhongqi Li (my3eee@126.com).

FIGURE 2. Schematic diagram of reverse series momentary coil structure

Designing and optimizing the physical structure of the coil is one of the most important measures to improve its resistance to deflection in order to reduce the impact of deflection. According to [12], a tower coil structure system is proposed to make the coil consumable less by a smaller receiving coil. However, a too small coupling coefficient leads to inefficient transmission of the system and insufficient distance of coil offset. To tackle the issue of inadequate offset resistance, [13] suggests a robust offset-resistant wireless charging system based on a DDQ/DD coupling mechanism and a two-way LCC/S compensation topology. This system employs fewer compensating components and demonstrates strong offset resistance. However, the coupling between the coils is not sufficient, which leads to a lower system transmission efficiency. To tackle this issue, [14] proposes a scheme in which the coil size does not exceed 400 mm, and the system transmission efficiency can still be maintained at a high level, but the system's offset resistance is insufficient, leading to considerable transmission efficiency fluctuations during the horizontal offset of the transmitting coil. Based on the above problems, [15] proposes a multi-coupling LCC compensation method for an electric vehicle dynamic wireless charging (EVDWC) system based on an integrated magnetic coupler. This method ensures higher system transmission efficiency while achieving quasi-constant efficiency, but the ability of compatibility with different load resistances is insufficient and corresponds to poor performance when the load changes. To address the problem of insufficient load compatibility, the wireless power transmission system proposed in [16] has some compatibility with load variations, but the transmission system also suffers from insufficient anti-skew performance. Based on the above factors, a constant voltage compensation network was proposed in [17], which makes the system resistant to offsets and at the same time shows some compatibility with load variations, but the voltage frequency of the system is 200 kHz, which exceeds the limit of 90 kHz stipulated by "SAE J2954". In the use of relay coils to improve the overall system offset resistance, the offset range in many existing reserches generally does not exceed 20% of the coil size, and the magnetic coupler transmits less power [18]. In the literature on enhancing the system's ability to withstand load fluctuations, most references achieve this by optimizing the topology of the circuit. However, references based on the coil structure are relatively scarce [19, 20].

To tackle these issues, this paper introduces a reverse series triple coil (RTC) structure, which is based on the traditional reverse tandem two-coil structure with fewer turns. As a result, the entire system achieves high transmission efficiency and strong anti-skewing capability, and increases load carrying capacity, to meet the growing demand for power in electric vehicles, smart devices, and other applications. In addition, this paper proposes an optimization method based on a reverse series triple coil structure by setting constraints and utilizes an ergodic algorithm to obtain coil parameters that satisfy the fluctuation rate of the coupling coefficients. Finally, the accuracy of the proposed structure and optimization method is validated through ANSYS Maxwell simulation and experimentation.
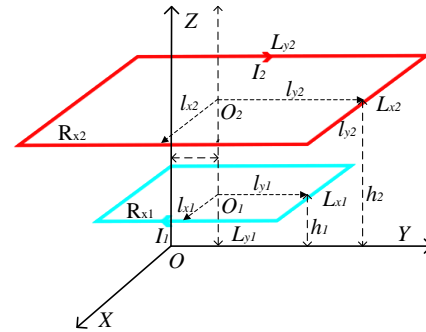
2. THEORETICAL CALCULATION OF RECTANGULAR COIL COUPLING COEFFICIENT

In this paper, in order to facilitate the optimization of the coupling coefficients of the proposed RTC structure, a method that allows for a fast calculation of the rectangular coil coupling coefficients is used. Firstly as shown in Figure 2, the vector magnetic potential expression proposed according to [21] is as follows.

$$\text{A}(x, y, z) = \frac{\mu_0}{4\pi} \int_\nu \frac{J(x', y', z')}{D_l} \tag{1}$$

where $\mu_0 = 4\pi * 10^{-7}$ is the magnetic permeability in air, J the current density, D_l the distance from a point on R_{x1} to any point on R_{x2} in space, and v the coil current distribution.

$$D_l = \sqrt{(x - x') + (y - y') + (z - z')} \tag{2}$$

To substitute the double Fourier transform and the inverse transform equation into (1), the transformed vector magnetic potential expression can be obtained.

$$a(\xi, \eta, z) = \frac{\mu_0}{2} \int_v e^{-j(x'\xi + y'\eta)} J(x', y', z') \frac{e^{-k|z - z_0|}}{k} dv' \tag{3}$$

In the case of a constant current distribution and a linear magnetic material, the flux density B_0 can be calculated using the following equation.

$$B_0 = \nabla \times A = ax \left(\frac{\partial Az}{\partial y} - \frac{\partial Ay}{\partial z} \right)$$
$$+ ay \left(\frac{\partial Ax}{\partial z} - \frac{\partial Az}{\partial y} \right) + az \left(\frac{\partial Ay}{\partial x} - \frac{\partial Ax}{\partial y} \right) \tag{4}$$

where ∇ is the Hamiltonian operator, and A denotes the vector magnetic potential. The following flux density expression is obtained after double Fourier transform operation and circuit analysis.

$$B_0 = \frac{1}{4\pi^2} \int_{-\infty}^{\infty} \int_{-\infty}^{\infty} C_i e^{-kz} e^{j(x\xi + y\eta)} d\xi d\eta \tag{5}$$

The following expression for the mutual inductance between coils can be obtained from the flux density B_0.

$$M_i = \frac{1}{4\pi^2 I} \int_{-\infty}^{\infty} \int_{-\infty}^{\infty} (C_z + C_x) \frac{e^{j(a_d + a)\xi} - e^{j(a_d - a)\xi}}{j\xi}$$

$$\cdot \frac{e^{j(b_d+b)\eta} - e^{j(b_d-b)\eta}}{j\eta} e^{-ks_2} \, d\xi d\eta \quad (6)$$

This in turn leads to the following equation for calculating the mutual inductance between multi-turn rectangular coils.

$$M = \sum_{m=1}^{N_a} \sum_{n=1}^{N_b} M_{mn} \quad (7)$$

where a_d and b_d are the offset distances from the x-axis and y-axis, respectively; N_a is the number of turns of R_{x1}; N_b is the number of turns of R_{x2}; m is the m-th turn of R_{x1}; and n is the n-th turn of R_{x2}. From [22], the rectangular coil self-inductance is calculated as follows .

$$
\begin{aligned}
L_i \;=\; & \frac{\mu_0}{\pi} N_i{}^2 \Bigg[a_i \ln \frac{2a_i b_i}{r_i \left(a_i + \sqrt{a_i{}^2 + b_i{}^2} \right)} \\
& + b_i \ln \frac{2a_i b_i}{r_i \left(b_i + \sqrt{a_i{}^2 + b_i{}^2} \right)} \\
& - 2 \left(a_i + b_i - \sqrt{a_i{}^2 + b_i{}^2} + \frac{1}{4} \left(a_i + b_i \right) \right) \Bigg] \quad (8)
\end{aligned}
$$

where N_i ($i = a$ or $i = b$) is the number of turns of coil winding; r_i is the radius of the rectangular average winding; and the rectangular length and width are a_i and b_i, respectively. The coil coupling coefficients can be further calculated according to Eqs. (7) and (8), and the coupling coefficients between the coils are calculated as follows.

$$k = \frac{M_{ab}}{\sqrt{L_a L_b}} \quad (9)$$

The coupling coefficients between the rectangular coils in equation can be calculated quickly by writing formulas using Matlab. This calculation method is faster than the ANSYS finite element simulation method and provides a theoretical basis for the design of coil parameters later.

3. RTC STRUCTURAL DESIGN

3.1. Coil Structure Analysis

Among the coil structures available for offset resistance, reverse series coils have a very streamlined coil structure, which makes it possible to meet the system's offset resistance while minimizing the use of materials. The rectangular reverse series coil structure is shown in Figure 3. Mutual inductive coupling effect is generated between the reverse series coil and transmitting coil by electromagnetic induction. Due to the existence of a part of the reverse series coil with an opposite direction of the winding of the transmitting coil, the mutual inductive coupling can offset part of the influence caused by the fluctuation of the magnetic field, so that the two coils have a stable mutual inductance between the two coils. Thus, their mutual coupling reduces the mutual inductance fluctuations of the coils as they move. With the advancement of wireless power transmission
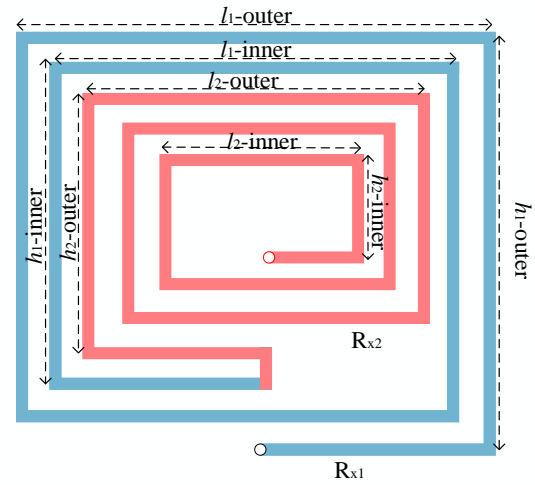

FIGURE 3. Reverse series coil structure diagram.

technology, various types of characteristics of relay coils have also been tapped, and the expected results obtained by adding relay coils at various locations in the wireless power transmission system vary. For instance, to obtain a high transmission efficiency in a three-coil wireless charging system, the distance between the primary coil and relay coil should be minimized. If a high output power is to be obtained from a three-coil wireless charging system, the distance between the primary and relay coils should be maximized. Under certain conditions, the inclusion of relay coils can adjust the inductance of the system, thus improving the system's compatibility with various loads. The structure of the three coils containing the relay is shown in Figure 4, where T_x represents the transmitting coil, R_l the relay coil, and R_x the receiving coil. The coil structure proposed in this paper combines the advantages of the reverse-series coil with those of the three-coil structure and makes further optimization to obtain an RTC structural system consisting of a short-orbit rectangular transmitting coil and two reverse-series rectangular coils, where one reverse-series coil serves as a relay coil, and the other reverse-series coil serves as a receiving coil. A mesh core structure made of ferrite is added to the top of the receiving coil and the bottom of the transmitting coil, respectively. The RTC structure is shown in Figure 5.
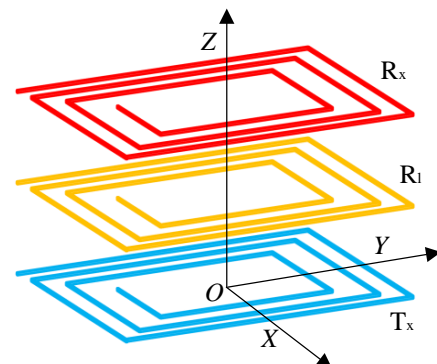

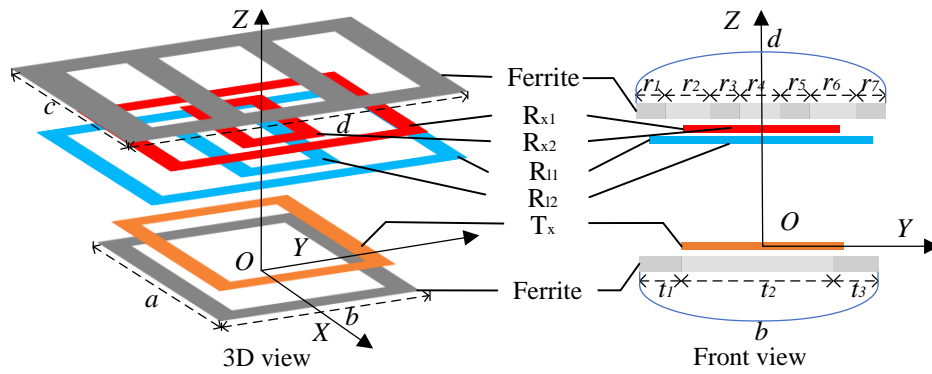**FIGURE 4**. Containing relay triple coil structure diagram.

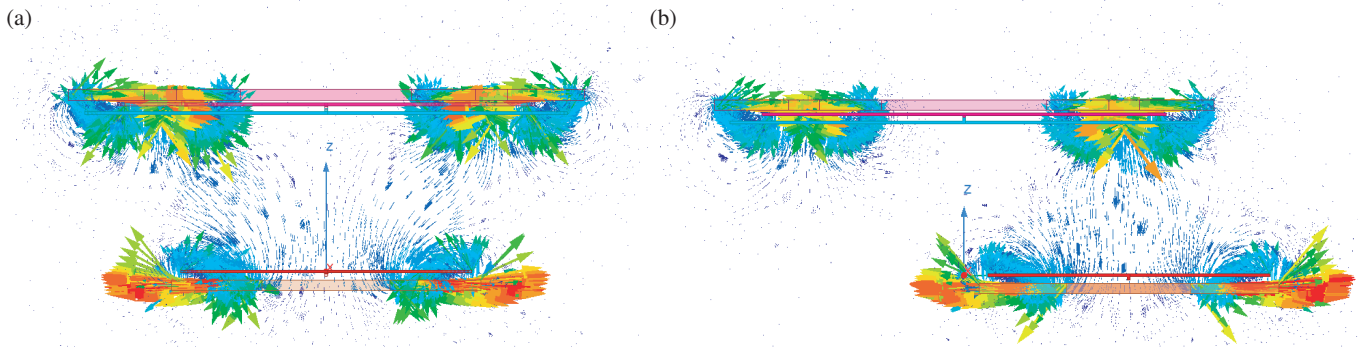**FIGURE 5**. RTC structure diagram.

FIGURE 6. RTC structure magnetic field distribution diagram.

One of the ferrites is the core structure, and the core can improve the system's coupling efficiency and enhance the magnetic field strength, while also providing a certain shielding effect. R_l1 is the relay's outer coil, and R_l2 is the relay's inner coil, which together form a reverse series relay coil that has the property of expanding the transmission distance, improving the transmission efficiency, or improving the load-carrying capacity under certain conditions. T_x is the transmitting coil, which utilizes a compact track coil structure that saves material while effectively avoiding magnetic leakage. R_x1 is the external receiving coil, and R_x2 is the internal receiving coil, which together form the reverse series receiving coil, and the coupling coefficient between them and T_x affects the overall transmission efficiency of the system and is crucial for its optimization. The core part adopts a type structure, and the simulation diagram of the RTC structure is obtained using Maxwell simulation software, placement of ferrite in areas of dense magnetic susceptibility distribution, while areas of sparse magnetic inductance are perforated to reduce the consumption of ferrite material and still retaining the high transmission efficiency of the coil. a and b are the length and width of the core portion of the transmitter coil; c and d are the length and width of the receiving coil. In order to ensure that the coil structure can have more application scenarios, the maximum size of all the coils proposed in this paper does not exceed 450 mm, and the distribution of magnetic field strength and magnetic inductance distribution of the coils is shown in Figure 6.

3.2. Mathematical Modeling Analysis of RTC Structure

The mathematical model of the RTC structure is Series-Series-Series topology (S-S-S topology circuit), which is a common way of connecting the circuits in a triple coil system. S-S-S topology circuits usually have high conversion efficiency because they use series connection, which employs fewer com-
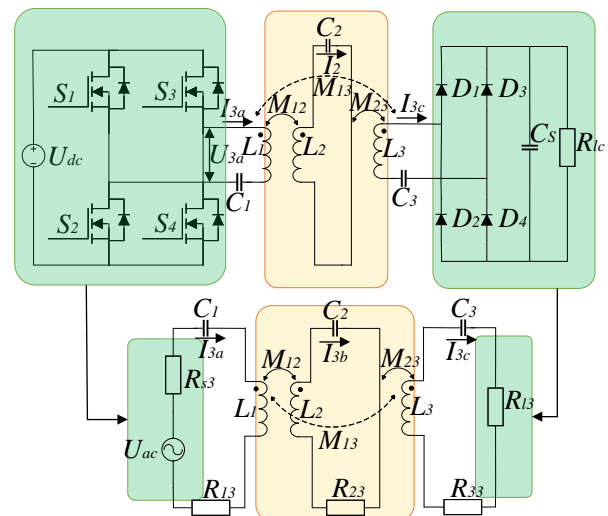

FIGURE 7. Mathematical modeling of the RTC structure.

ponents and reduces the power loss of the power supply during the conversion process. S-S-S topology circuits have good constant-current (CC) characteristics in single-supply power supply systems for wireless power transmission [23]. The mathematical model of the RTC structure is shown in Figure 7. In the figure, U_{dc} is the DC power supply; C_1, C_2, and C_3 are the resonant capacitors that resonate the inductors L_1, L_2, and L_3, respectively, and they are related to each other by $C_i = 1/(L_i \omega^2)$ $(i = 1, 2, 3)$. C_s is the compensation capacitor; U_{ac} and R_s are the equivalent AC power supply and internal resistance of the DC power supply U_{dc} and the inverter module; R_l is the equivalent resistance R_{lc} of the rectifier and the load resistor; and U_s represents the output voltage of the DC-AC inverter. In an S-S-S topology circuit, the mathematical expressions for U_{ac} and R_l are as follows.

$$U_{ac} = U_s + R_s I_a \tag{10}$$

$$R_1 = \left(2\sqrt{2}/\pi\right)^2 R_{lc} \tag{11}$$

M_{12} is the mutual inductance between the transmitting coil and relay coil, M_{13} the mutual inductance between the transmitting

coil and receiving coil, and M_{23} the mutual inductance between the relay coil and receiving coil. The S-S-S circuit WPT is analyzed according to Kirchhoff's voltage law (KVL), and the following equations are obtained.

$$\begin{bmatrix} \dot{U}_{ac} \\ 0 \\ 0 \end{bmatrix} = \begin{bmatrix} Z_1 & j\omega M_{12} & j\omega M_{13} \\ j\omega M_{12} & Z_2 & j\omega M_{23} \\ j\omega M_{13} & j\omega M_{23} & Z_3 \end{bmatrix} \begin{bmatrix} \dot{I}_a \\ \dot{I}_b \\ \dot{I}_c \end{bmatrix} \tag{12}$$

Among them:

$$\begin{cases} Z1 = R_l + R_s + j\omega L_1 + j\omega C_1 \\ Z2 = R_2 + j\omega L_2 + j\omega C_2 \\ Z3 = R_3 + R_l + j\omega L_3 + j\omega C_3 \end{cases} \tag{13}$$

The currents in the circuits where T_x, R_l, and R_x are located can be calculated as shown in Eq. (15).

$$I_1 = \frac{U_S(jM_{23}{}^2\omega^2 + Z_2 Z_3)}{Z_3 M_{12}{}^2\omega^2 - 2jM_{12}M_{13}M_{23}\omega^3 + Z_2 M_{13}{}^2\omega^2 + Z_1 M_{23}{}^2\omega^2 + Z_1 Z_2 Z_3}$$

$$I_2 = \frac{jU_S\omega(M_{13}M_{23}\omega + jM_{13}Z_3)}{jZ_3 M_{12}{}^2\omega^2 + 2M_{12}M_{13}M_{23}\omega^3 + jZ_2 M_{13}{}^2\omega^2 + jZ_1 M_{23}{}^2\omega^2 + jZ_1 Z_2 Z_3} \tag{14}$$

$$I_3 = \frac{jU_S\omega(M_{13}Z_2 - jM_{12}M_{23}\omega)}{Z_3 M_{12}{}^2\omega^2 - 2jM_{12}M_{13}M_{23}\omega^3 + Z_2 M_{13}{}^2\omega^2 + Z_1 M_{23}{}^2\omega^2 + Z_1 Z_2 Z_3}$$

Let $\omega M_{12} = A$, $\omega M_{13} = B$, $\omega M_{23} = C$, and the expression for the efficiency of the S-S-S triple coil structure is obtained:

$$\eta = \frac{R_l(BZ_2 - jAC)^2}{(C^2 + Z_2 Z_3)(A^2 Z_3 + B^2 Z_2 + C^2 Z_1 - 2jABC + Z_1 Z_2 Z_3)} \tag{15}$$

Z_1, Z_2, and Z_3 in the resonant state are regarded as constants, which are brought into Eq. (15), and the relationship between mutual inductance and efficiency between the coils is obtained by solving for the value of the maximum value function in the interval in Matlab: The magnitude of the transmitting coil and relay coil mutual inductance M_{12} is proportional to the transmission efficiency, and the magnitude of the relay coil and receiving coil mutual inductance M_{23} is proportional to the magnitude of the relay coil. The mutual inductance M_{13} of the transmitting and receiving coils is inversely proportional to the transmission efficiency. When the mutual inductance and coupling coefficient between the transmitting coil and receiving coil are close to 0, the RTC system has the highest transmission efficiency, at which point $B = 0$. The simplified formula is shown in (16).

$$\eta = \frac{R_l(AC)^2}{(C^2 + Z_2 Z_3)(A^2 Z_3 + C^2 Z_1 + Z_1 Z_2 Z_3)} \tag{16}$$

4. RTC SYSTEM DESIGN AND OPTIMIZATION

4.1. Coil Parameterization

For the WPT system with a single relay coil of the S-S-S topology circuit, the effect of cross-coupling will cause the power in the system to be transferred to each other between the coils, thus affecting the efficiency of the system's power transfer. It is known from the literature [24] that the condition for ignoring the effect of cross-coupling for a three-coil system in an S-S-S topology circuit is:

$$k_{13}{}^2 Q_S Q_L \ll 1 \tag{17}$$

Among them:

$$\begin{aligned} Q_S &= \omega L_1/R_s + R_1 \\ Q_L &= \omega L_3/R_l + R_3 \end{aligned} \tag{18}$$

That is, in line with the previous conclusion that the size of the mutual inductance M_{13} of the transmitting and receiving coils is inversely proportional to the transmission efficiency, since M_{13} tends to 0, then it can be judged that the system does not
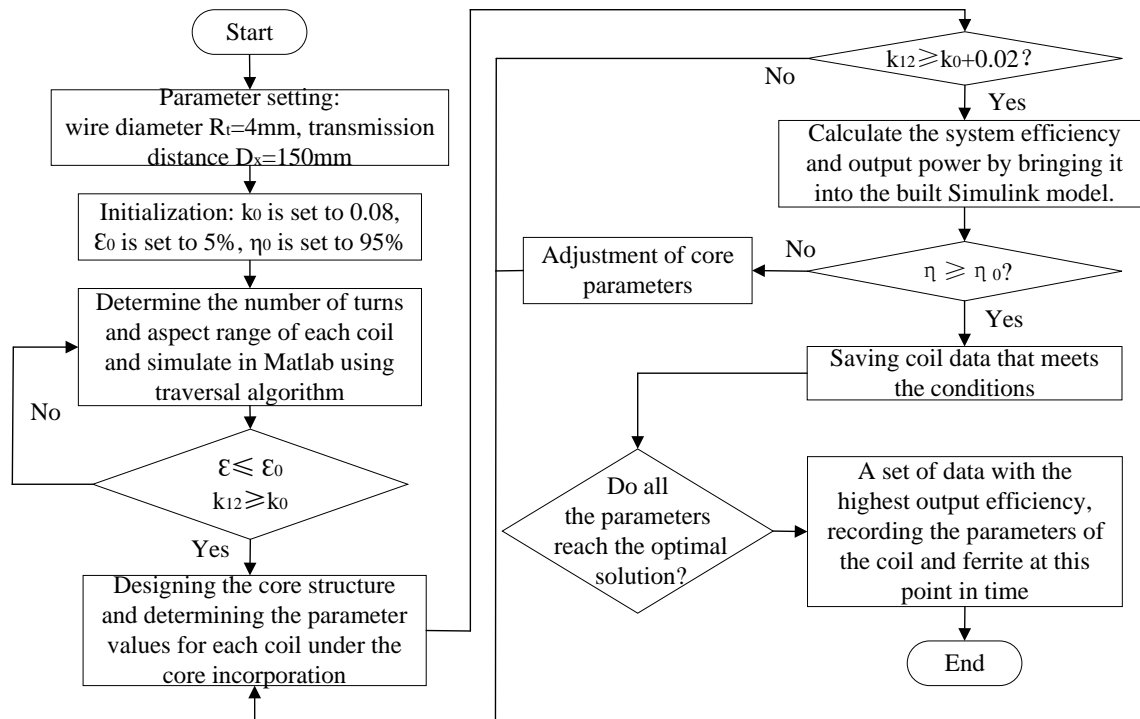
FIGURE 8. Coil structure optimization process.

have cross-coupling to the system's transmission efficiency. As the mutual inductance M_{23} of the relay coil and receiver coil increases the system transmission efficiency also increases, but as M_{23} increases it also makes the optimal load resistance larger, so the value of M_{23} is limited by the load resistance R_l. In existing automotive wireless power transmission systems, the equivalent resistance of electric vehicle loads is common between $15\,\Omega$ and $50\,\Omega$ [16, 17], and the range of M_{23} can be constrained based on this characteristic.

So to ensure the efficiency of the RTC system, the mutual inductance value and the coupling coefficient between the transmitter coil and receiver coil need to be reduced, then the receiver coil can be made to converge to 0 with the mutual inductance M_{13} of the transmitter coil by reversing the series coil structure. As the mutual inductance M_{23} of the relay coil and receiver coil increases, the system transmission efficiency also keeps on increasing, but as M_{23} increases it also makes the optimum load resistance larger, so the value of M_{23} is limited by the load resistance R_{l3}. In existing automotive wireless power transmission systems, the equivalent resistance of electric vehicle loads is generally between $15\,\Omega$ and $50\,\Omega$ [29, 30], and the range of M_{23} can be constrained according to this characteristic. To satisfy the high transmission efficiency, the constraint of mutual inductance between the coils is: First, the mutual inductance M_{12} of the transmitter coil and the relay coil is as large as possible. Second, the mutual inductance M_{13} of the transmitting and receiving coils tends to zero. Finally, the mutual inductance M_{23} between the relay coil and receiving coil at the value corresponding to the highest system transmission effi-

ciency when the load resistance varies between $15\,\Omega$ and $50\,\Omega$.

To make the value of the mutual inductance M_{13} between the receiving coil and transmitting coil tend to 0, the receiving coil can be connected in reverse series structure, and the corresponding parameters of the inner and outer layers of the receiving coil can be adjusted to decouple with each other and the transmitting coil, so that the mutual inductance M_{13} between them tends to 0. After the receiving coil is determined to be a reverse series structure, in order to ensure that the value of M_{23} is as large as possible, the relay coil can adopt a structure similar to that of the receiving coil, that is, it adopts the form of a reverse series rectangular coil, so as to make the direction of the magnetic coupling between the relay coil and the receiving coil the same, and to ensure that the value of M_{23} is as large as possible. While the size of the coupling coefficient between the transmitting coil and relay coil is directly proportional to the system transmission efficiency, in the reverse series coil, increasing the coupling coefficient between the two coils will lead to an increase in the mutual inductance fluctuation rate, so we can write the mutual inductance Eq. (7) and self-inductance Eq. (8) mentioned above into Matlab for calculating and filtering the size of the coils by traversing optimization method, and the detailed optimization flow is shown in Figure 8.

(1) Parameter setting and initialization: the longitudinal transmission distance between the T_x and R_l is set to 150 mm; the gap between the R_l and R_x is 4 mm; the diameter of the copper wire is 4 mm; and the settings are $k_0 = 0.08$, $\varepsilon_0 = 5\%$, and $\eta_0 = 95\%$.

TABLE 1. Parameters of coils.

Coils	Inner length/cm	Inner width/cm	Outer length/cm	Outer width/cm	Turns
T_x	34.6	17.8	44.2	27.4	12
R_{l1}	37.4	37.4	45.0	45.0	10
R_{l2}	31.8	19.6	37.0	24.8	7
R_{x1}	37.6	37.6	38.8	38.8	2
R_{x2}	32.6	19.6	34.6	21.6	3

(2) Setting constraints: Setting the maximum size of the outer coil of R_l to be less than 450 mm, and the size of T_x to be greater than or equal to 60% of the outer coil size. The R_x is kept decoupled from the T_x; the number of turns of the coil is set in steps of 1 turn; and the edge length of the coil is set in steps of 1 mm. The optimal coil parameters are obtained by traversing the algorithm and calculating it in Matlab.

(3) Determine whether the mutual inductance fluctuation rate ε is less than ε_0, and k_{12} is greater than 0.08. If all the above conditions are met, the design of the core structure based on the coil parameters is started; otherwise, reuse the traversal algorithm to perform the calculation in Matlab.

(4) The magnetic field distribution diagram of the RTC system is obtained by Maxwell simulation software, and the magnetic core is made into a mesh shape and placed in the position where the magnetic inductance is dense. The values of the RTC system with magnetic core are obtained through simulation, and the obtained data are brought into the Simulink model to calculate the system efficiency and transmission power.

(5) Condition judgment: in order to meet the higher transmission efficiency of the RTC system, it is necessary to meet the coupling coefficient k_{12} of the T_x, and the intermediate coil is greater than or equal to 0.1. If the condition is met, the output of the resulting RTC structural system efficiency will be simulated by Simulink, and it will be judged whether the efficiency of the RTC structural system at this point in time is not lower than 95% of the system parameters. If the result meets the above two conditions, the result will be saved; otherwise, the result will not be saved, and the optimization of coil parameters will continue. If all coil parameters reach the upper limit, end the mutual inductance optimization procedure; otherwise, the procedure jumps back to the coil optimization session.

(6) Output the solution found: Save and output the result that satisfies all the set conditions.

The optimal coil size parameters are obtained through the above optimization link, and the detailed coil size parameters are shown in Table 1. The distribution of magnetic inductance in space is obtained through Maxwell software simulation to get the optimum primary edge core size corresponding to the values in Figure 4 as $a = 500$ mm, $b = 290$ mm, $t_1 = t_3 = 85$ mm, and $t_2 = 120$ mm. The dimensions of the optimal secondary core side correspond to the values $c = 480$ mm, $d = 500$ mm, $r_1 = r_7 = 72$ mm, $r_2 = r_6 = 30$ mm, $r_3 = r_5 = 60$ mm, and $r_4 = 160$ mm. The thickness of the core of the coupling mechanism is designed as a mesh-type ferrite core with a thickness of 10 mm, which saves material and ensures efficiency, while allowing the coil to have a quasi-constant effect in the event of a horizontal deflection.

4.2. RTC System Frequency Optimization

In Eq. (16), both A and C are determined by the coil structure itself, which can be further analyzed to show the effect brought by the change of power supply frequency and horizontal offset on the efficiency. The specific steps are as follows: firstly, each size parameter of the optimized coil is plotted in Maxwell software, and then the data of mutual inductance, self-inductance, and internal resistance obtained by simulation are brought into (16) to obtain the transmission efficiency of the RTC system, and finally, set the horizontal offset step and system frequency step to obtain a graph showing the impact of frequency and horizontal offset on efficiency.

Take the horizontal Y-axis offset of the transmitting coil as ΔD_x and the length of the ferrite core at the bottom of the transmitting coil as D_{Tx}, so that $D* = \Delta D_x / D_{Tx}$, then $D*$ is the horizontal Y-axis offset rate of the transmitting coil. As can be seen in Figure 9, the transmission efficiency of the system based on the reverse series coil as the relay coil increases with the increase of frequency. In order to meet the requirements of "SAE J2954", the charging frequency of the electric vehicle battery ranges from 79 kHz to 90 kHz, and this paper chooses 90 kHz as the frequency of power supply with the highest gain in transmission efficiency for the RTC structure. In this paper, we choose 90 kHz as the frequency of the power supply, which has the highest gain for the transmission efficiency of the RTC structure system. From the effect of different frequency changes on the transmission efficiency of the system during the variation of $D*$, it can be concluded that the change of frequency does not affect the quasi-constancy of the transmission efficiency of the system in the horizontal Y-axis offset.

5. RTC STRUCTURE SIMULATION AND EXPERIMENTAL VERIFICATION

5.1. Experimental Platform Construction

In order to verify the rationality of the design of the RTC structural system, 0.1 mm × 800 strands of Leeds wire were used to wind the coil, and the coil parameters shown in Table 1 were used in the winding process for the design. The acrylic sheet is used as a filler between the gaps of the coils. The thickness of the acrylic sheet is consistent with the diameter of the coils 4 mm thickness, and it has good insulating properties to
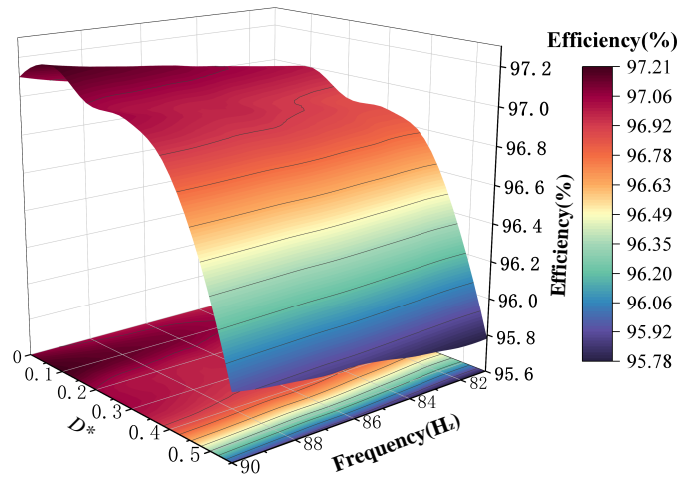
FIGURE 9. Effect of erequency and horizontal Y-axis offset on efficiency.
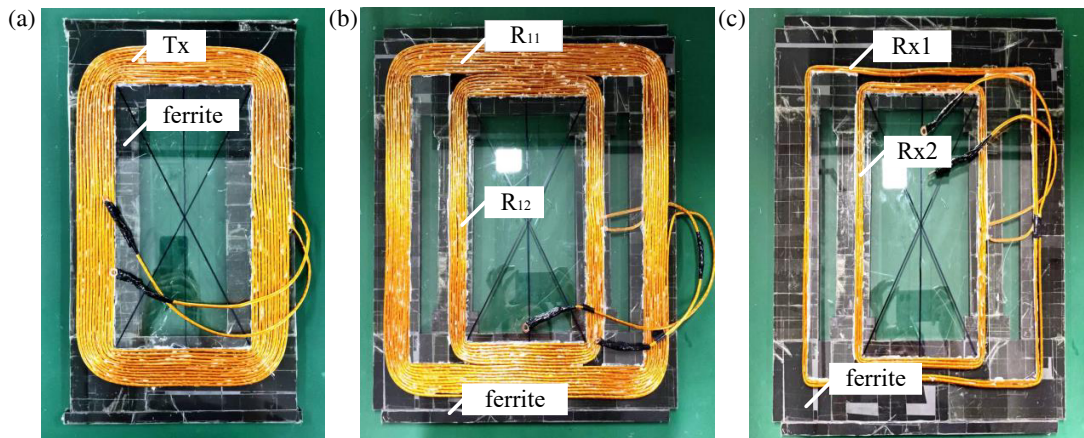

FIGURE 10. RTC physical drawing. (a) Transmitting coil. (b) Relay coil. (c) Receiving coil.

avoid power loss and leakage, where the physical models of the transmitting coil, relay coil, and receiving coil are shown in Figure 10.

After the coils are wound, the values of self-inductance, mutual inductance, and equivalent internal resistance are measured; the measured data are recorded; and the transmitting, relaying, and receiving coils are connected according to the S-S-S topology circuit shown in Figure 7 to build the WPT experimental platform shown in Figure 11. The cores have a mesh design and are placed below the transmitter coil and above the receiver coil.

The WPT circuit system is constructed by Simulink simulation, and the experimental construction is carried out according to the circuit built in Simulink simulation. In this WPT circuit system, the system parameters of each device in the WPT circuit system are obtained according to the parameter optimization method, and the system parameters of each device of the coreless coil structure are obtained as shown in Table 2. The system parameters of each device of the core-coil structure are shown in Table 3.

5.2. RTC Structure Simulation and Experimentation

During the experiment, the self-inductance and mutual inductance values between the coils are obtained by the impedance analyzer, and the self-inductance and mutual inductance values are brought into Eq. (19) to obtain the coupling coefficients between the coils measured by the experiment.

$$k = \frac{M}{\sqrt{L_1 L_2}} \tag{19}$$

The mutual inductance values and coupling coefficients measured experimentally are compared and analyzed with the simulated values obtained from ANSYS Maxwell simulation, and the relationship between the mutual inductance values and coupling coefficients during the horizontal offset of the transmitting coil is plotted. The mutual inductance values and coupling coefficients of the RTC system without a core under the horizontal offset are shown in Figure 12, and those of the RTC system with a magnetic core are shown in Figure 13.
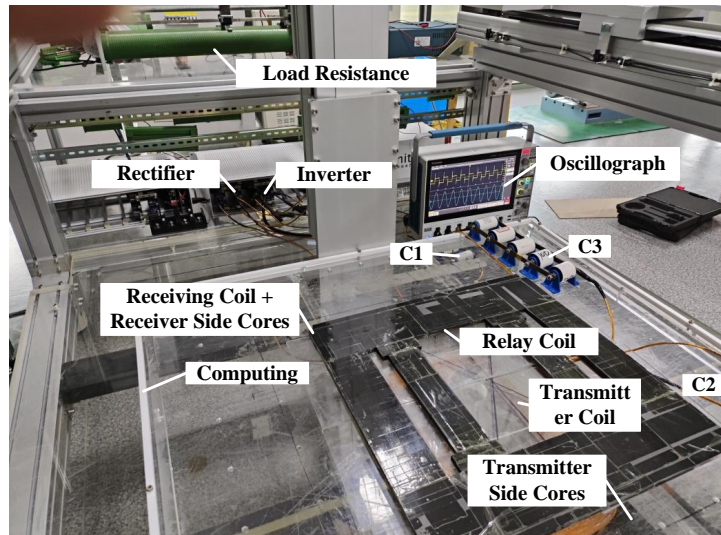
FIGURE 11. WPT experimental system.

TABLE 2. Experimental parameters of the RTC structure (Core-less).

Parameter	Physical meaning	Value
$L_1/\mu H$	Self-inductance of the transmitting coil	89.17
$L_2/\mu H$	Self-induction of relay coils	92.61
$L_3/\mu H$	Self-inductance of the receiving coil	9.26
C_1/nF	Compensation capacitance of the transmitter coil	35.07
C_2/nF	Compensation capacitance for relay coils	33.77
C_3/nF	Compensation capacitance of receiving coil	337.71
$C_f/\mu F$	Output Filter Capacitor	50
f_0/kHz	Working frequency	90
R_L/Ω	Load Equivalent Resistance	19

**TABLE 3**. Experimental parameters of the RTC structure (cores available).

Parameter	Physical meaning	Value
$L_1/\mu H$	Self-inductance of the transmitting coil	138.39
$L_2/\mu H$	Self-induction of relay coils	123.54
$L_3/\mu H$	Self-inductance of the receiving coil	12.50
C_1/nF	Compensation capacitance of the transmitter coil	22.60
C_2/nF	Compensation capacitance for relay coils	25.31
C_3/nF	Compensation capacitance of receiving coil	250.18
$C_f/\mu F$	Output Filter Capacitor	50
f_0/kHz	Working frequency	90
R_L/Ω	Load Equivalent Resistance	19

From the various data of mutual inductance values and coupling coefficients obtained from Figure 12 and Figure 13 under horizontal offset, it can be seen that the mutual inductance values and coupling coefficients firstly increase and then decrease with the increase of horizontal distance, and the mutual inductance volatility can be further obtained after obtaining the data as shown in (20):
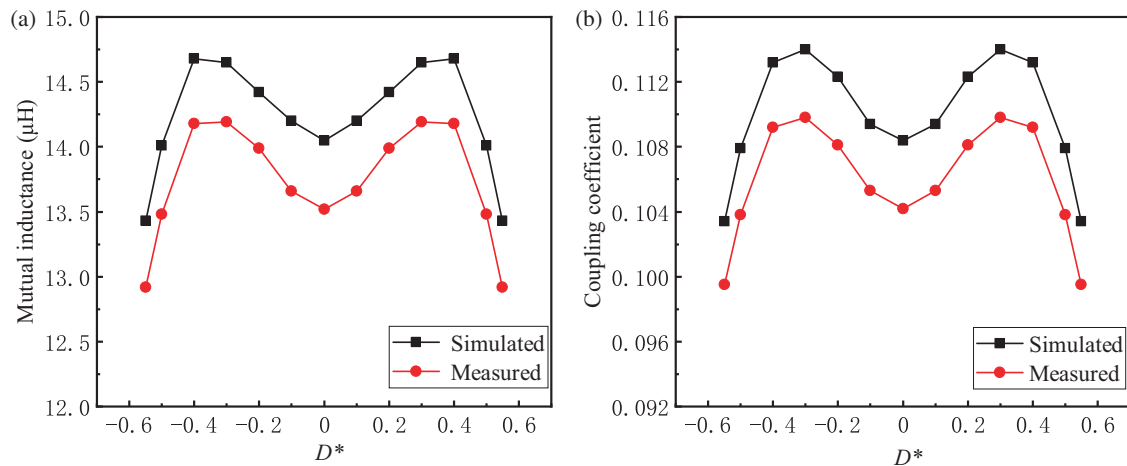
$$\varepsilon = \left| \frac{M_{X0} - M_{XL}}{M_{X0}} \right| \times 100\% \qquad (20)$$

where ε is the mutual inductance fluctuation rate, M_{X0} the mutual inductance value when no offset occurs, M_{XL} the mu-
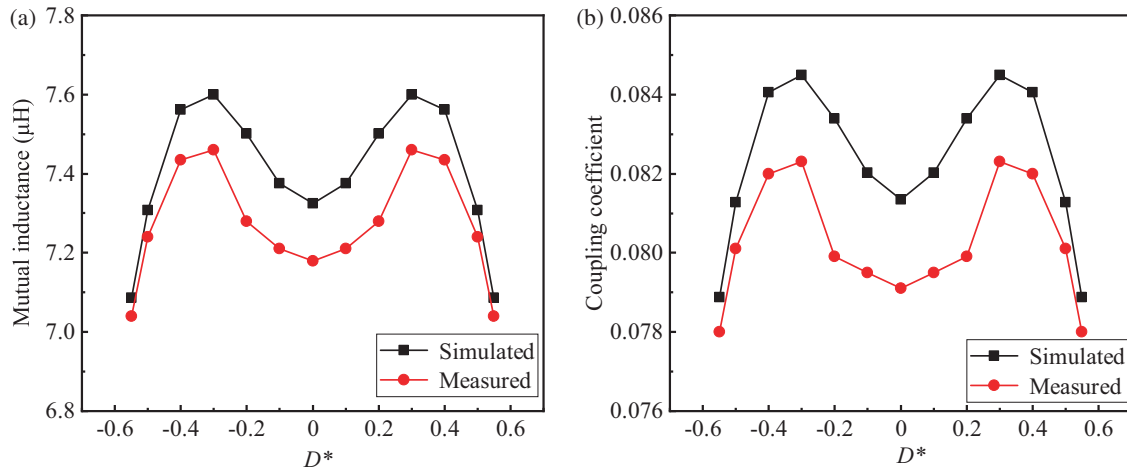
FIGURE 12. Mutual inductance values and coupling coefficients for transmitting coils offset along the horizontal Y-axis (Core-less). (a) Mutual inductance value at Y-axis offset. (b) Coupling coefficients under y-axis offset.


FIGURE 13. Mutual inductance values and coupling coefficients for transmitting coils offset along the horizontal Y-axis (cores available). (a) Mutual inductance value at Y-axis offset. (b) Coupling coefficients under y-axis offset.

tual inductance value after offset, and the step distance is set to 2.5% of the horizontal length, in which the mutual inductance fluctuation rate of the transmitting coil and relay coil of the coreless RTC structure reaches a maximum of 4.69% at a horizontal offset of 30%, and reaches 30% at a horizontal offset of 55% (148.5 mm). The mutual inductance fluctuation between the transmitter coil and relay coil of the core specific RTC structure reaches a maximum of 4.89% at 30% horizontal offset and 4.45% at 55% horizontal offset, and neither of them exceeds the 5% mutual inductance fluctuation at a distance of 55% (159.5 mm) from the offset transmitter coil. With the input and output power obtained from the experiments, the efficiencies of the magnetic coreless RTC structure and the magnetic core RTC structure are calculated when they are in each position, as shown in Figure 14 for the system transmission efficiency of the magnetic core structure and the magnetic coreless structure at different offset distances. It can be seen that adding optimized cores to a coil system can make the system transmission more efficient. The maximum efficiency fluctuation point

of the coreless RTC structure is 0.82% at a distance of 20% horizontal offset, with a maximum efficiency of 92.89%. The maximum efficiency fluctuation point of the RTC structure with magnetic core is 1.19% at a distance of 55% horizontal offset, and the maximum efficiency is 97.26%. The distance at which the fluctuation rate of the cores structure fluctuates at a horizontal offset of 55% of the length is increased by the expansion of the core to the transmitting coil, which has a longer transmission distance, a factor that inevitably leads to greater efficiency fluctuation rate of the cores RTC structure.

In order to verify the strength of the three-coil structure and the two-coil structure with the load capacity, the two structures were connected using the circuit built in Figures 6 and 7, respectively, through the varistor module to make the load resistance change, record the load from $15\,\Omega$ to $80\,\Omega$ under the change in the corresponding values, the values obtained through the plotting software to draw the relationship between the load resistance value and the efficiency of the graph shown in Figure 15.
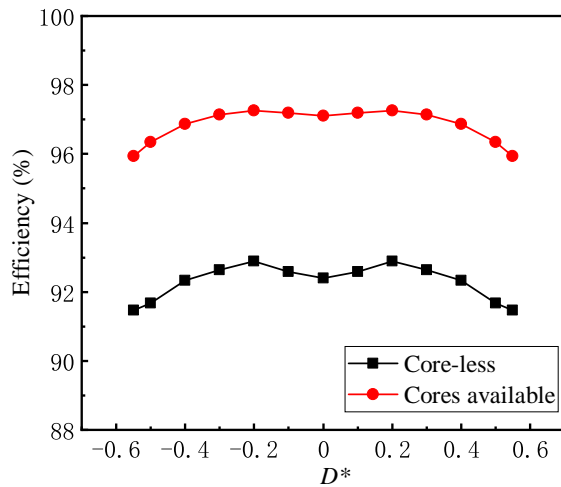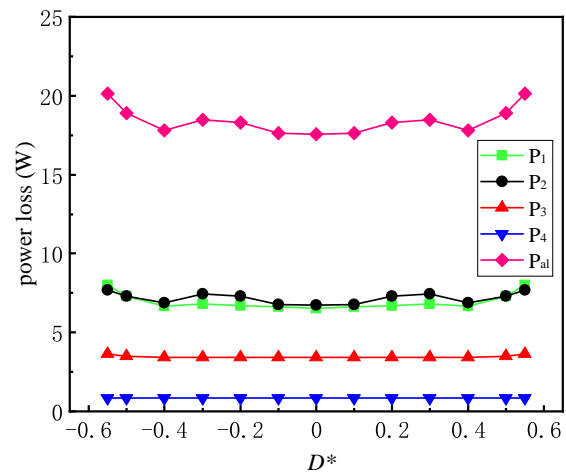
FIGURE 14. Efficiency plot of coreless structure vs. core structure during horizontal Y-axis deflection.
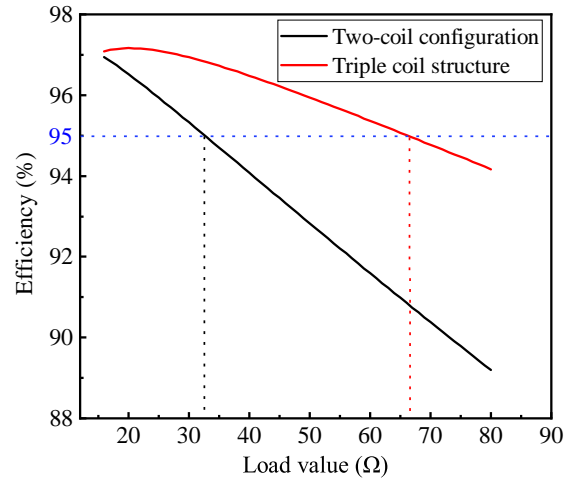
FIGURE 15. Efficiency plot with varying load resistance.
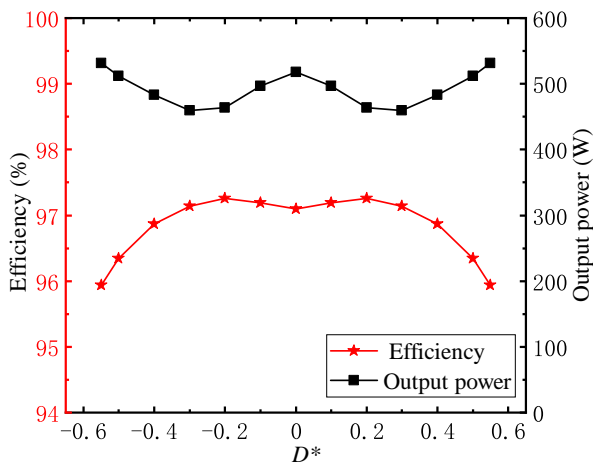
FIGURE 16. RTC coil transfer efficiency and output power at Y-axis offset.

FIGURE 17. Analysis of major internal resistance losses in RTC structured circuit systems.

It can be seen from Figure 15 that the transmission efficiency of the system with the three-coil structure will be consistently higher than that of the system with the two-coil structure in the interval after $15\,\Omega$. With the gradual increase of the load resistance value, the system transmission efficiency in the dual-coil structure decreases rapidly to below 95% after the load resistance reaches $32\,\Omega$. The load resistance of the three-coil structure reaches $68\,\Omega$ before the system transmission efficiency slowly decreases to less than 95%, which shows that in terms of load-bearing capacity, the three-coil structure has a more stable system transmission efficiency than the two-coil structure when the load changes, and it is more adaptable to more automotive power supply in the wireless power transmission system.

According to Figure 16, the relationship between the output power and transmission efficiency of the wireless power transmission system during the horizontal offset and the offset distance can be derived. Under the power supply with a frequency

of $90\,\text{kHz}$ and an input power of $520\,\text{W}$, the highest efficiency occurs at the position of 20% of the width of the core of the offset transmitting coil in a horizontal distance of 55% of the total length of the offset transmitting coil, and the transmission efficiency of the system at this time is 97.26%. The system output power loss during the offset process is all within $21\,\text{W}$, with very low power loss. The system transmission efficiency is almost always above 96%, which meets the constant efficiency standard for dynamic wireless charging during automobile movement.

5.3. RTC Structure Loss Analysis

In the process of analyzing WPT circuits, each device itself will inevitably have internal resistance due to material or structural factors. To obtain the power losses, the losses in each branch of the circuit and the equivalent internal resistance losses at different receiver locations were calculated and plotted in Figure 17.

TABLE 4. Comparison of experimental parameter performance in literature.

References	Size of Tx (L×W)	Size of Rx (L×W)	Maximum offset distance	Load range	Maximum transmission efficiency	Maximum efficiency volatility
[13]	550 mm∗550 mm	350 mm∗350 mm	150 mm	/	88.35%	0.96%
[14]	240 mm∗240 mm	240 mm∗240 mm	100 mm	/	94.29%	3.7%
[16]	400 mm∗400 mm	400 mm∗400 mm	/	15 Ω–25 Ω	95.79%	1.66%
our work	442 mm∗274 mm	450 mm∗450 mm	159.5 mm	15 Ω–68 Ω	97.26%	1.19%

'/' denotes that the value is not given in the references. (Length × width) is abbreviated as ($L \times W$)

In the figure, P_1, P_2, P_3, and P_4 are the power consumed by the parasitic internal resistance of the transmitting coil, the parasitic internal resistance of the relay coil, the parasitic internal resistance of the receiving coil, and the parasitic internal resistance of the power supply, respectively, and P_{al} is the total system power loss. When the input voltage of the system is 65 V, and the input current is 8 A, the total power loss of the system during the process of offsetting the transmitting coil by 55% of its own horizontal distance is almost always below 20 W, and the system power loss fluctuates less during the offsetting process. The overall efficiency of the system is quasi-constant. The results show that the total power loss in the circuit is very small.

5.4. Comparative Analysis of Experimental Parameters

The performance comparison between the RTC structure and the other structures presented in the references is shown in Table 4. In order to simulate the condition of identical coil dimensions, each wireless energy transmission system is normalized. Let the maximum coil offset distance of each wireless energy transmission system be $W_{\max}$, and the length of the transmitting coil in the horizontal motion direction of the car be L_f. Let $\lambda = W_{\max}/L_f$, then λ in [13] and [14] are 0.27 and 0.42, respectively, and the value of λ in the RTC structure proposed in this paper is 0.58, while the coil structure in [16] has no offset resistance by itself. Therefore, under the condition of the same simulated coil size, the RTC structure has higher anti-offset capability than other wireless energy transmission systems. In terms of transmission efficiency, the RTC structure has stronger load carrying capacity and higher transmission efficiency and more stable efficiency fluctuation rate. The system transmission efficiency of the RTC structure remains almost constant without any auxiliary equipment.

6. CONCLUSION

In this paper, an RTC structure is proposed, and the novel structure consists of a short-track rectangular transmitting coil and two reverse-series rectangular coils. One of the reverse-series coils serves as a relay coil, while the other reverse-series coil serves as a receiving coil. The feasibility of the proposed method is demonstrated by the proposed optimization method based on the reverse series triple coil structure using Maxwell with experimental validation. The experimental results indicate that, without adding other topology structures and com-

pensator components, and under the premise that the system transmission efficiency is not lower than 95%, compared to the traditional reverse series-connected two-coil structure, the RTC structure has a stronger load-bearing capacity. Its load-bearing capacity is 300% higher than that of the traditional reverse series-connected two-coil structure. In the process of horizontal Y-axis offset transmitter coil core width of 55% of the distance (159.5 mm), the maximum efficiency fluctuation rate is 1.19%, ensuring that the system's transmission efficiency can reach a nearly constant maximum of 97.26%.

REFERENCES

[1] Yan, H., Y. Chen, and S.-H. Yang, "UAV-enabled wireless power transfer with base station charging and UAV power consumption," *IEEE Transactions on Vehicular Technology*, Vol. 69, No. 11, 12 883–12 896, 2020.

[2] Triviño, A., J. M. González-González, and J. A. Aguado, "Wireless power transfer technologies applied to electric vehicles: A review," *Energies*, Vol. 14, No. 6, 1547, 2021.

[3] Cirimele, V., R. Torchio, J. L. Villa, F. Freschi, P. Alotto, L. Codecasa, and L. D. Rienzo, "Uncertainty quantification for SAE J2954 compliant static wireless charge components," *IEEE Access*, Vol. 8, 171 489–171 501, 2020.

[4] Cirimele, V., J. Colussi, J. L. Villa, A. L. Ganga, and P. Guglielmi, "Modelling of a 100 kW–85 kHz three-phase system for static wireless charging and comparison with a classical single-phase system," in *2020 IEEE International Symposium on Circuits and Systems (ISCAS)*, 1–5, 2020.

[5] Zhang, Y., S. Chen, X. Li, and Y. Tang, "Design of high-power static wireless power transfer via magnetic induction: An overview," *CPSS Transactions on Power Electronics and Applications*, Vol. 6, No. 4, 281–297, 2021.

[6] Bagchi, A. C., A. Kamineni, R. A. Zane, and R. Carlson, "Review and comparative analysis of topologies and control methods in dynamic wireless charging of electric vehicles," *IEEE Journal of Emerging and Selected Topics in Power Electronics*, Vol. 9, No. 4, 4947–4962, 2021.

[7] Tan, L., W. Zhao, H. Liu, J. Li, and X. Huang, "Design and optimization of ground-side power transmitting coil parameters for EV dynamic wireless charging system," *IEEE Access*, Vol. 8, 74 595–74 604, 2020.

[8] Cai, C., M. Saeedifard, J. Wang, P. Zhang, J. Zhao, and Y. Hong, "A cost-effective segmented dynamic wireless charging system with stable efficiency and output power," *IEEE Transactions on Power Electronics*, Vol. 37, No. 7, 8682–8700, 2022.

[9] Li, Z., X. Xiong, L. Ren, P. Kong, Y. Zhang, and J. Li, "Design and optimization of quasi-constant coupling coefficients for superimposed dislocation coil structures for dynamic wireless charging of electric vehicles," *Progress In Electromagnetics Research M*, Vol. 116, 23–38, 2023.

[10] Duong, T. P. and J.-W. Lee, "A dynamically adaptable impedance-matching system for midrange wireless power transfer with misalignment," *Energies*, Vol. 8, No. 8, 7593–7617, 2015.

[11] Yuan, Z., Q. Yang, X. Zhang, X. Ma, R. Wang, M. Xue, and P. Zhang, "A misalignment tolerate integrated S-S-S-compensated WPT system with constant current output," *Energies*, Vol. 16, No. 6, 2798, 2023.

[12] Li, Z., M. Zhang, S. Huang, and J. Yi, "Design and optimization of structure of tower-type coil in wireless charging system for electric vehicles," *Progress In Electromagnetics Research B*, Vol. 85, 85–101, 2019.

[13] Zhuang, T. and Y. Yao, "A DDQ/DD-coupler-based wireless power transfer system for electric vehicles charging featuring high misalignment tolerance," in *Proceedings of the CSEE*, Vol. 42, 5675–5684, 2022.

[14] Shi, H. and W. Li, "Research on coil parameter optimization and misalignment characteristics of wireless charging system," *Journal of Hefei University of Technology (Natural Science)*, Vol. 44, No. 9, 1179–1186, 2021.

[15] Shi, K., C. Tang, H. Long, X. Lv, Z. Wang, and X. Li, "Power fluctuation suppression method for EV dynamic wireless charging system based on integrated magnetic coupler," *IEEE Transactions on Power Electronics*, Vol. 37, No. 1, 1118–1131, 2022.

[16] Jie, R. and Y. Liu, "Study on anti-misalignment inductive power transfer system based on parameter optimized method," *Proceedings of the CSEE*, Vol. 39, 1452–1460, 2019.

[17] Mai, J., Y. Wang, Y. Yao, and D. Xu, "Analysis and design of high-misalignment-tolerant compensation topologies with constant-current or constant-voltage output for IPT systems," *IEEE Transactions on Power Electronics*, Vol. 36, No. 3, 2685–2695, 2021.

[18] Cheng, S. and Y. Wang, "Anti-misalignment characteristics of wireless charging magnetic coupler with large relay coil," *Electric Power Automation Equipment*, Vol. 43, 213–219, 2023.

[19] Bui, D., Q. Zhu, L. Zhao, and A. P. Hu, "Concentric-coil hybrid IPT system with improved tolerance to coupling and load variations," *IEEE Journal of Emerging and Selected Topics in Power Electronics*, Vol. 10, No. 4, 4913–4922, 2022.

[20] Lu, Y., B. Yang, S. He, Y. Peng, T. Lyu, R. Mai, and Y. Chen, "Design of compensation topology for IPT system considering coils' parameters and load variations for CC or CV output," *IEEE Transactions on Transportation Electrification*, Vol. 10, No. 1, 1583–1595, 2023.

[21] Li, Z. and S. Li, "Mutual inductance calculation and optimization of multi-receiver positive and negative series coil structure in dynamic wireless power transfer systems," *Transactions of China Electrotechnical Society*, Vol. 36, 5153–5164, 2021.

[22] Yıldırız, E., "Optimal design with generalized inductance calculation for IPTs using a spiral rectangular coil pair," *Electric Power Components and Systems*, Vol. 50, No. 19-20, 1212–1222, 2022.

[23] Zhang, Y., Z. Shen, W. Pan, H. Wang, Y. Wu, and X. Mao, "Constant current and constant voltage charging of wireless power transfer system based on three-coil structure," *IEEE Transactions on Industrial Electronics*, Vol. 70, No. 1, 1066–1070, 2023.

[24] Luo, B. and W. Li, "Cross-coupling effects and reactance compensation for radio energy transmission in magnetically coupled resonant triple coils," *Electric Power Automation Equipment*, Vol. 39, 105–112, 2015.